

# Femto-second laser texturing prediction using COMSOL Multiphysics®

E.C. Chevallier<sup>1</sup>, V. Bruyère<sup>1</sup>, G. Bernard<sup>2</sup>, P. Namy<sup>1</sup>

<sup>1</sup>: SIMTEC, Grenoble, France

<sup>2</sup>: GFMS, Meyrin, Switzerland

## 1. Introduction

Surface engineering is a key technology used in a wide range of sectors in industry. Among other techniques, it involves adding functionality to a surface. This can be performed by creating a specific topography to a surface using laser texturing. Laser surface texturing (LST) has emerged as a promising texturing technique due to properties such as excellent repeatability, non-contact process, the ability to achieve small-size features and high-quality finishing. Even though LST is a mature process, already available through a number of machine tool suppliers, its commercial applications are mainly limited to decorative rather than functional texturing.

The work described here is part of the H2020 research programme called SHARK (PID: 768701) which aims at developing laser surface texturing from the current trial-and-error, lab-scale concept to a highly predictable, finite element (FE) modelling and data driven industrial approach. One of the challenges of the SHARK project is to overcome the lack of knowledge and resources available to inform the laser parameters selection. In this paper, the focus is on topography prediction after ultra-short pulse laser impacts. Femto-second laser texturing offers the possibility to reduce significantly the amount of molten material [1]. This means better surface properties as well as more accurate prediction of the surface topography.

The aim of the work presented in this paper is to develop a model that captures the important physical phenomena involved in the femto-second laser texturing process. The ultra-short energy deposition leads to a non-equilibrium temperature state taken into account through a Two-Temperature model, described in more details in the following section. The heat transfer was implemented and coupled with some matter ablation in a 2D cartesian model. In this model, a range laser parameters such as overlap and average

power were tested. The influence on the final crater topography is presented and discussed.

## 2. Physical phenomena involved during a femtosecond laser pulse

### Physical phenomena

In the femto-second laser-matter interaction, the pulse duration is smaller than the time required for the temperature to reach equilibrium and the “classic” temperature modelling approach cannot be used. In fact, as presented in Figure 1, the heating process can be separated in two phases. The first phase corresponds to the electron to electron scattering time and is of the order of magnitude of tens of femtoseconds. During this phase, the energy is firstly absorbed by the electrons but not by the lattice. The second phase, of several tens of picoseconds, corresponds to the energy transfer from the electrons to the subsystem.

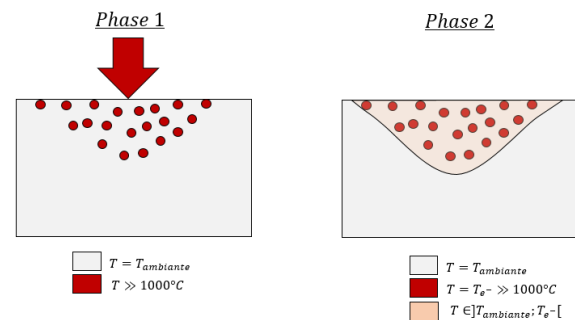


**Figure 1:** Energy transmission phases of the femto-second laser source to the lattice.

## 3. Ultra-short laser pulse duration: need for the two temperature model

In this section, the equation solved when solving the two-temperature model are presented. The model is implemented using COMSOL Multiphysics® for a range of pulse durations. The idea behind this is to

identify the need for a two-temperature model for ultra-short pulses.

### Model geometry

The FE model presented in this work was developed with COMSOL Multiphysics® version 5.4. A 2D geometry and a time-dependent study are considered.

### Thermal problem: the Two-Temperature model

The model described in literature to take into account this separation of the two time period is called the “Two Temperature model”. It consists in a continuous model used to describe the time evolution of the temperatures of the sub-systems by coupled differential equations [2]:

$$\rho_e C_e \frac{\partial T_e}{\partial t} = \nabla [k_e \nabla(T_e)] - \kappa(T_e - T_l) + S(x, t)$$

$$\rho_l C_l \frac{\partial T_l}{\partial t} = \nabla [k_l \nabla(T_l)] + \kappa(T_e - T_l)$$

Where  $T$  is the temperature of the system, subscripts  $e$  and  $l$  denotes the electrons and the lattice respectively.  $C, \rho$  and  $k$  are the specific heat capacity, mass density and thermal conductivity.  $\kappa$  is the electron-phonon coupling constant and  $S(x, t)$  is the laser source term.

The energy deposition is assumed to be Gaussian and is modelled by a boundary heat flux. The thermal inward heat flux is formulated as:

$$-\mathbf{n} \cdot (-k_l \nabla T) = P_{laser} \cdot \frac{A_0}{\pi \left(\frac{w_0}{2}\right)^2} \cdot e^{-\frac{r^2}{\left(\frac{w_0}{2}\right)^2}}$$

where  $P_{laser}$  is the peak laser power,  $A_0$ , the surface absorptivity,  $r$ , the radius and  $w_0$ , the beam waist.

The peak laser power is computed from the average power  $P_{ave}$  and the power time distribution  $f_{deposition}$  is the power time distribution (unit-less quantity), represented by a rectangle function:

$$f_{deposition}(t) = \begin{cases} 1 & \text{if } t \in [0, \tau_{laser}] \\ 0 & \text{if } t > \tau_{laser} \end{cases}$$

where the pulse duration is referred to as  $\tau_{laser}$ . As the average power is the average of the laser power over a period,  $P_{laser}$  should satisfy the following equation:

$$P_{ave} \cdot \frac{1}{f} = \int_{t \in [0, \frac{1}{f}]} P_{laser} \cdot f_{deposition}(t) dt$$

where  $f$  the frequency of the laser pulses and

On the other boundaries of the model, thermal insulation is assumed, by forcing the normal conductive flux to be null:

$$-\mathbf{n} \cdot (-k \nabla T) = 0$$

### Mesh

A mapped (regular) mesh of quadratic elements is used in the refined region where the laser source is deposited, whereas a quadrilateral coarser mesh is used elsewhere. The size of the elements in the small region is set as large as possible to reach reasonable computing time yet fine enough to capture the temperature gradient.

### Material properties

The simulation presented in this paper is performed considering an AISI 316L austenitic stainless steel, a well-known material widely used in industry. The material properties and laser input parameters used in the model are reported in Table 1 and Table 2 respectively. The lattice thermal properties were averaged with temperature values from [3]. The electron thermal properties have no physical meaning here and were obtained from the author through a calibration (not detailed in this paper) allowing the observation of the physical phenomena of the femtosecond laser pulse as described in [1], i.e.

- Electron temperature reaches several tens of thousands of Kelvin
- Electron to electron scattering time of several tens of femtoseconds
- Electron to phonon scattering time of several picoseconds

**Table 1:** Thermal material properties used in the model.

Designation	Symbol	Value used in the model
Mass density of the lattice	$\rho_l$	$8000 \text{ kg m}^{-3}$
Thermal conductivity of the lattice	$k_l$	$30 \text{ W m}^{-1} \text{ K}^{-1}$
Specific heat of the lattice	$C_l$	$600 \text{ J kg}^{-1} \text{ K}^{-1}$
Electron-phonon coupling constant	$\kappa$	$10^{17} \text{ W m}^{-3} \text{ K}^{-1}$

Surface absorptivity	$A_0$	0.5
Mass density of the electron *	$\rho_e$	$8000 \text{ kg m}^{-3}$
Thermal conductivity of the electron *	$k_e$	$3 * 10^8 \text{ Wm}^{-1}\text{K}^{-1}$
Specific heat of the electron *	$C_e$	$6 * 10^5 \text{ Jkg}^{-1}\text{K}^{-1}$

**Table 2:** Laser input parameters used in the model.

Designation	Symbol	Value used in the model
Laser beam size	$w_0$	$30 \mu\text{m}$
Average power	$P_{ave}$	0.7 W
Laser power during the pulse	$P_{laser}$	$\approx 4 * 10^9 \text{ W}$
Pulse duration	$\tau$ or tau	From $100 \text{ fs to } 100 \text{ ns}$
Frequency of laser pulses	$f$	1 kHz

#### Time dependent solver

The scales involved in the process vary from femtoseconds (during the laser pulse) to tens of microseconds (duration of one period) which causes the problem to be multi-scale in time. This requires a careful setup of the time step during the resolution, especially when the gradient of the heat flux deposited with time is large, i.e. at the beginning of the impact. During the impact, the time step is fine enough to capture this (ultra-short) deposition, as well as the two phases described in the first paragraph of this section. Then, when the material cools down, the time step is increased to avoid excessively long computational times, as the ratio of the cooling time over pulse duration is typically 1:10-100.

## 4. Two temperature model results for a range of laser pulse durations

### Electron and lattice temperature evolution during a femtosecond laser pulse deposition

The model was tested on a range of pulse durations from 100 fs to 100 ns. In Figure 2, the temperature of the lattice (green) and that of the electrons (blue) are presented, along with the pulse duration (red). The top image represents the evolution of the electron and lattice temperatures for a duration of 50 ps whereas the bottom image is a zoom in on the temperatures evolution during 200 fs, i.e. twice the duration of the laser impact simulated. The electrons are heated as the laser energy is deposited as it can be seen on the bottom image in Figure 2 since the electron energy absorption timescale is of the order of magnitude of femtoseconds. The electron temperature rises up to 50000 K. The energy is then transferred to the lattice. The electron and lattice temperature reach the same value after approximately 30 ps. At this stage, the hypothesis of a continuous description of temperature becomes valid again.

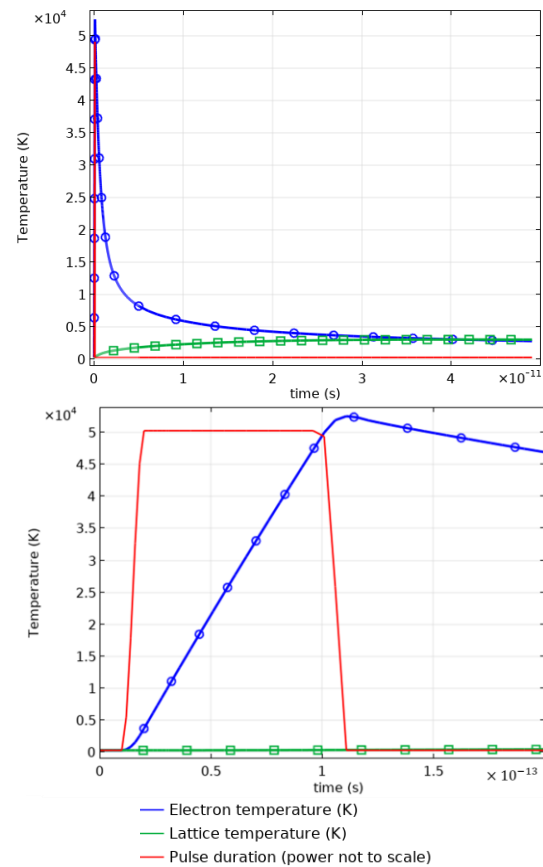


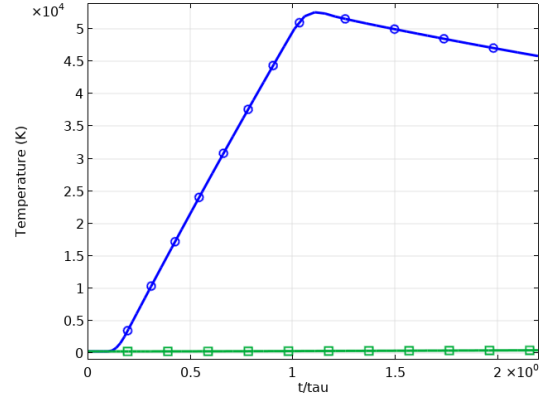
**Figure 2:** Electron and lattice temperature evolution during the laser impact of 100 fs.

From femtosecond to nanosecond laser impact simulations: identification for the need to use the two-temperature model

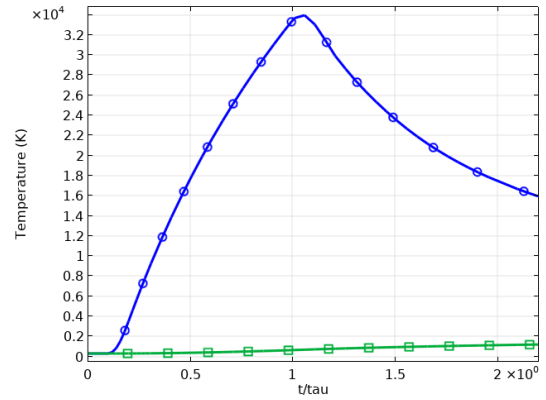
The model described in the previous section was used to simulate laser impact for a range of pulse durations. It should be noted that the only difference between models presented in this section is the laser pulse duration  $\tau$ , the material properties and other laser inputs are kept identical for the temperature evolution comparison.

In the images presented in Figure 3 from a to g, the electron and lattice temperatures are presented against  $t/\tau$  as this scale allows comparing the temperature evolutions for different laser pulse durations. The temperatures are observed for a duration of two laser impacts so the diffusion from the electron to the lattice can be observed. For laser pulses of 100 fs to 10 ps, the electron and lattice temperature are different of more than an order of magnitude and the diffusion time from electron to lattice is larger than twice the pulse duration. For a laser pulse duration of 100 ps, the ratio between electron and lattice temperatures is less than 2, and the diffusion time from the electrons to the lattice is about twice the laser pulse duration. For laser pulses of 1 ns and longer, the electron and lattice temperatures coincide well. In Figure 4, the ratio of the electron temperature over the lattice temperature is presented. For laser pulses of 10 ps and shorter, the ratio is larger than 10, whereas for laser pulses of 1 ns and larger, the ratio is lower than 1.5. From these figures, it can be concluded that the use of the two-temperature model is required for laser pulses of 10 ps and less.

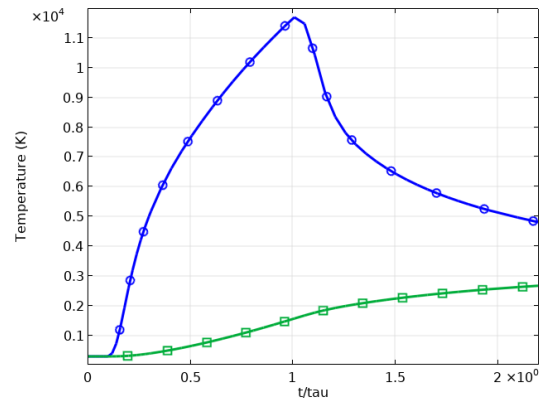
In the graphs presented in Figure 3, it can be noticed that the maximum temperature is decreasing with the pulse duration. This is expected as the laser parameters are unchanged from one case to another, hence the average power  $P_{ave}$  and the frequency  $f$  are fixed. The laser power is computed as described in the second paragraph of section 3, i.e. a longer pulse duration causes a lower laser power during the peak.



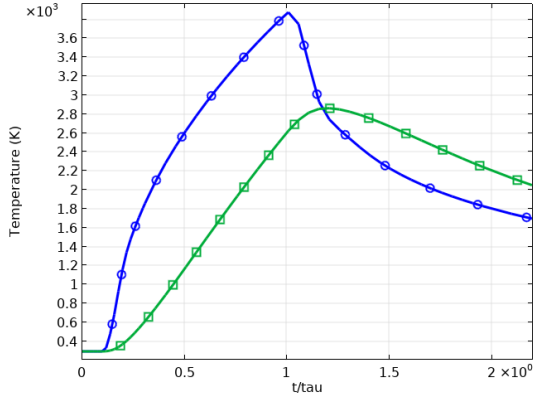
(a)



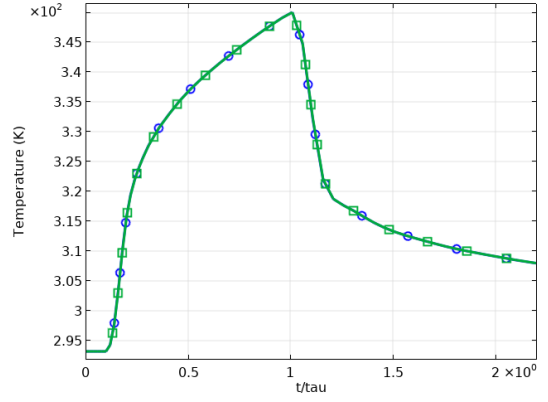
(b)



(c)

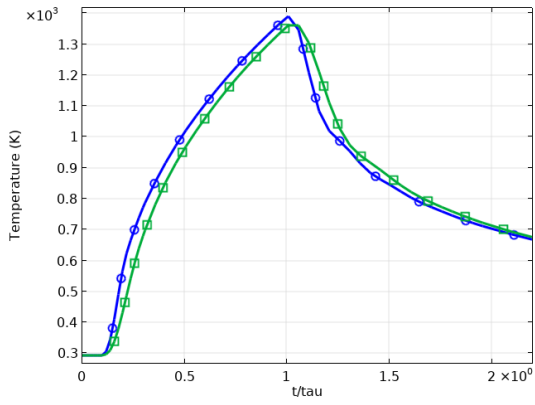


(d)

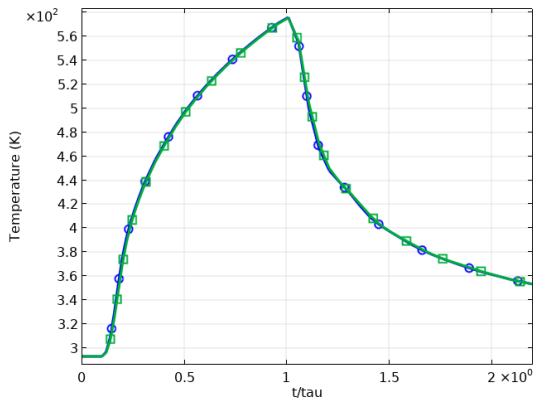
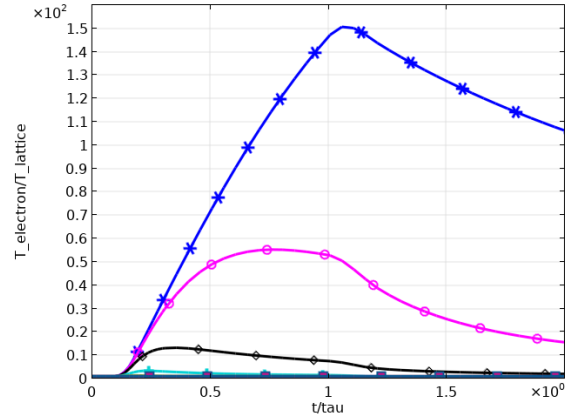


(g)

**Figure 3:** Electron and lattice temperature evolution during laser impacts of 100 fs (a), 1 ps (b), 10 ps (c), 100 ps (d), 1 ns (e), 10 ns (f) and 100 ns (g)



(e)



(f)

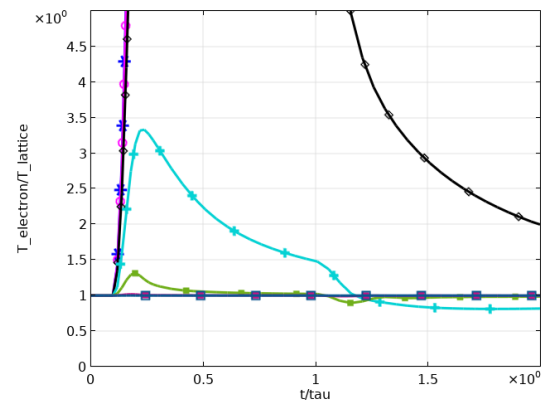


**Figure 4:** Ratio of the electron temperature over the lattice temperature for a range of laser pulse simulations (top). Zoom on the results obtained for lower pulse durations (bottom).

## 5. Application of the two temperature model on laser ablation examples

The model developed to simulate ultra-short laser pulses was used to simulate laser ablation. The topography of the crater after matter removal is obtained at the end of the simulation using the moving mesh technique. The laser ablation modelling is presented in the following sections.

### Ablation modelling

In this model, only the solid phase is modelled meaning the gas around the component and the vaporised matter are not simulated. This choice of modelling also implies the mass is not conserved. In order to compute the shape of the solid component after one laser impact, the assumption that the solid material surface temperature not exceeding the vaporisation temperature  $T_{vap}$ . In the model, this assumption is expressed by the use of the convective flux boundary condition defined as:

$$\Phi_{vap} = h(T - T_s)$$

where  $\Phi_{vap}$  is the vaporised flux,  $h$  is a numerical parameter.

At the solid gas interface, the energy balance is assumed and is expressed as:

$$\rho L_v \mathbf{u}_{vap} \cdot \mathbf{n} = \Phi_{vap} \cdot \mathbf{n}$$

where  $L_v$  is the latent heat of vaporization,  $\mathbf{u}_{vap}$ , the velocity of the matter leaving the interface and  $\mathbf{n}$  the normal vector of the solid front.

The surface is considered free to move to accommodate the change in geometry due to the matter loss. The Deformed Geometry interface is used by setting the normal mesh velocity  $v_n$  at the solid gas interface to:

$$v_n = \Phi_{vap} / (\rho * L_v)$$

### Moving mesh

At each time-step, the displacement of the moving boundary is propagated throughout the domain using Laplace mesh smoothing technique which minimises the displacement difference between two neighbour nodes.

### Results

Figure 5 presents a sequence of 12 femto-second laser impacts divided in three rows of four impacts. Each of them creates a crater, but the shape of the crater highly depends on the topology created by the previous impacts. The model enables to account for the thermal evolution of the material and the cumulated effect of

the different impacts. According to the specificities of this type of laser, the resulting crater is very smooth allowing for precise applications. Given the application of interest, parameters such as the average power, period duration, overlap and distribution of the impacts are selected to produce the appropriate final crater topology.

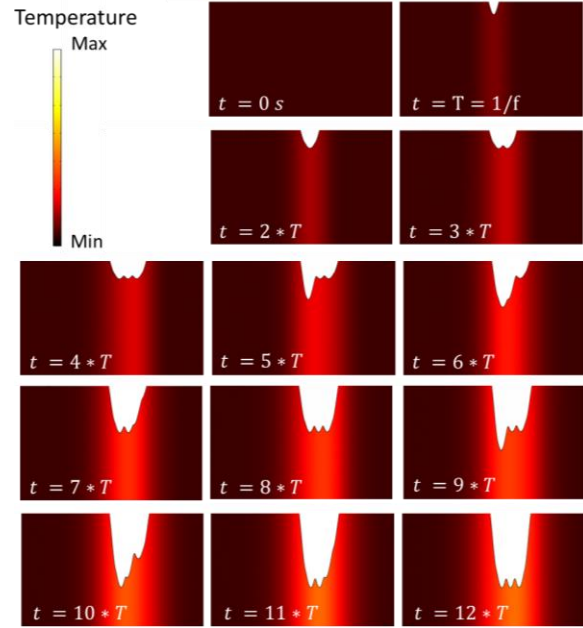


Figure 5: Multi-impact ablation progression

## 6. Conclusions

After introducing the “Two Temperature Model” and including it in an FEM model dedicated to laser femto-second ablation, the work presented in this paper highlighted the influence of the modelling choices at different time scales. The results presented confirms the need to use the model that distinguishes electron and lattice temperature for the simulation of the laser matter interaction involving laser pulses shorter than 10 ps.

The model developed integrates and couples:

- a modelling energy exchange between the electrons and the lattice
- a thermal modelling adapted to the time scale,
- a modelling of the evaporation rate on the impacted surface,
- a moving mesh to consider the surface modifications due to evaporation.

Thanks to an appropriate single impact modelling, it is possible to make predictions on the shape of a single impact crater but also of a multi-impact crater. The modelling of a single ultra-short pulse is hardly of

interest for industries, however, this step is required to understand the physical phenomena occurring during one laser impact. Further work on the model would include the development and experimental validation of the prediction of the topography produced after hundreds of ultra-short laser impacts.

## **7. Acknowledgements**

This project has received funding from the European Union's Horizon 2020 Framework Programme for research and innovation under grant agreement no 768701.

## **8. References**

1. K.-H. Leitz, B. Redlingshöfer, Y. Reg, A. Otto and M. Schmidt, Metal ablation with short and ultrashort laser pulses, *Physics Procedia*, **12**, 230-238 (2011)
2. P. Ji and Y. Zhang, Multiscale modelling of femtosecond laser irradiation on copper film with electron thermal conductivity from *ab initio* calculation, *Numerical Heat Transfer Applications*, **71(2)**, (2016)
3. S. K. Bate, R. Charles and A. Warren, Finite element analysis of a single bead-on-plate specimen using SYSWELD, *International Journal of Pressure Vessels and Piping*, **86**, 73-78 (2009)